Self-assembled biodegradable block copolymer precursors for the generation of nanoporous poly(trimethylene carbonate) thin films

Nikola Toshikj, Jason Richard, Michel Ramonda, Jean-Jacques Robin, Sebastien Blanquer

Version of Record: https://www.sciencedirect.com/science/article/pii/S0032386123002100
Manuscript_2e69cbc338fa33588b2f6c69792d2dcd

Self-assembled biodegradable block copolymer precursors for the generation of nanoporous poly(trimethylene carbonate) thin films

Nikola Toshikj[1], Jason Richard[2], Michel Ramonda[3], Jean-Jacques Robin[1], Sebastien Blanquer[1]*

1 ICGM, Univ Montpellier, CNRS, ENSCM, Montpellier, France

2 IEM, Univ Montpellier, ENSCM, CNRS, Montpellier cedex 5, Montpellier F-34095, France

3 Centrale de Technologie en Micro et Nanoélectronique, Univ Montpellier, Campus Saint Priest, CC 05013, 860, rue de St Priest, 34095, Montpellier Cedex5, France

KEYWORDS

biodegradable block copolymers, phase separation, nanoporous thin films, PTMC, poly(DL-lactide), PLA, photo-crosslinking, solvent vapor annealing

ABSTRACT

Even though the domain of nanoporous template manufacturing from self-assembled block copolymers is in full expansion, challenging studies addressing innovative biodegradable block copolymer assemblies are still not reported. Herein, we address the usage of an original biodegradable precursor to prepare nanoporous thin films: the PTMC-*b*-PDLLA-*b*-PTMC triblock copolymer. The copolymer is designed to have a favorable interaction parameter for phase-separation, which was confirmed by differential scanning calorimetry by the appearance of two distinctive glass transition temperatures, corresponding to each of the blocks. Thin films are firstly produced by spin-coating and two methods are investigated for achieving organized self-assembly of the system: solvent evaporation and solvent vapor annealing. Well-organized bicontinuous nanoscopic phase-separated morphologies consisting of PTMC and PDLLA domains are achieved under precise solvent vapor annealing conditions for a particular triblock copolymer composition. Triblock copolymer self-assembly is compared to the one occurring in PTMC/PDLLA blends where no ordered phase-separation is observed. Moreover, thin films photo-crosslinking of previously methacrylated PTMC end-blocks, beneficial to the stability and cohesion of the PTMC phase, as well as mechanical strength of the porous matrix, proved to preserve the phase separation. From the optimal oriented block copolymer thin films, selective etching *via* PDLLA mild hydrolysis resulted in nanoporous PTMC with maintained long-range

order and stability. Such approach to generate nanoporous PTMC could have great potential in both biomedical applications and the energy field.

1. Introduction

Recently, the usage of organic porous materials has greatly increased for energy (heterogeneous catalysis and storage), environmental (adsorption/separation processes) and medical (drug delivery and regenerative medicine) applications.[1, 2] Among varied precursors, the block copolymers (BCPs) have demonstrated remarkable versatility in manufacturing functional nanoporous structures.[2-4] Their ability to phase-separate in ordered morphologies within 10-200 nm range derives from the thermodynamic incompatibility between the blocks and is governed by the BCP composition and their molecular masses.[5, 6] Hence, three parameters directly influence the microphase separation: the Flory-Huggins interaction parameter (χ), the volume fraction of the minority block (f), as well as the degree of polymerization (N). The dimensionless χ-value designates the incompatibility between the differing blocks, whereas the segregation product χN shapes out the degree of microphase separation. Thus, particular attention was accorded in the literature to these parameters in the area of BCP phase-separation.[7, 8]

In the frame of porous nanostructure engineering, we evidence an expansion of the BCP assemblies where the minority block organizes into porogenic nanophases while the majority component acts as mechanically robust framework supporting the voids.[9] Therefore, dating from 1988, the selective removal of an etchable polymer component from a self-assembled system has been throughout examined toward the “bottom-up” generation of nanoporous monoliths and thin films.[10] In most cases, poly(styrene) (PS) is imposed as the porous matrix,

since this polymer favors effective phase-separation and imparts good mechanical properties. Thus, various di-, tri- or multiblock copolymer precursors have been reported to deliver nanoporous PS. Going forward, the first introduction of a biodegradable block in the research area of nanoporous thin films was made possible *via* poly(styrene)-poly(lactide) copolymers.[11, 12] Hence, several precursors containing semi-crystalline or amorphous poly(lactide) as an etchable component have been reported until now.[13, 14] Nevertheless, the challenge of developing a fully biodegradable block copolymer self-assembly leading to a porous matrix remained. In fact, introducing nanopores within a biodegradable polymer would open a new vision to the concept of nanoporous materials. As such, the (nano)porous components can be used as sustainable engineering devices in various domains of application, altogether with low environmental impact and absence of by-products.

Consequently, motivated by the necessity to explore contemporary self-assembled BCP associations and above all oriented towards the biodegradable BCPs as the future of polymer materials,[15] we investigated the likely phase-separation leading to nanoporous thin films from such systems. Two important factors influenced the selection of our biodegradable BCP: the Flory-Huggins interaction parameter (calculated by the Hoftyzer – Van Krevelen method) together with the prerequisite of a differing biodegradability of the blocks regarding selective etching. Hence, we focused our research on amorphous polymers where the poly(trimethylene carbonate)/poly (D,L-lactic acid) (PTMC/PDLLA) system particularly attracted our attention.

PTMC is a biodegradable and biocompatible amorphous elastomer presenting high flexibility at room temperature.[16] PTMC photo-crosslinking leads to a mechanical stable network, paving the way toward additive manufacturing techniques.[17, 18] In addition, PTMC is the perfect candidate for a tunable and programmable degradability, due to its sensible nature

by surface erosion in a precisely selected enzymatic environment.[16] On the other hand, amorphous PDLLA is known to display a rapid degradation rate undertaking a hydrolytic bulk erosion mechanism, thus being promoted as a fitting candidate for an etchable block.[19] From the literature, the couple of material PTMC/PDLLA have been already reported as membranes where the non-cytotoxicity, biodegradability and biocompatibility of these materials have been recognized to be a notable advance in the field.[20-22] However, neither self-assembled structures due to the incompatibility of the two components nor an organized porosity has been investigated in these cases.

In the aim to investigate the phase-separation in the PTMC/PDLLA system, we focused on PTMC-*b*-PDLLA-*b*-PTMC triblock copolymers. A triblock copolymer structure was preferred over diblock one in order to anticipate the nanoporous matrix stabilization by further crosslinking of the PTMC moieties after their end-functionalization by methacrylate groups. Thus, at the beginning of the study, the synthesized triblock copolymer has been analyzed by differential scanning calorimetry (DSC) and atomic force microscopy (AFM) techniques in the aim of investigating its phase-separation. Later, the capacity of the system for the generation of nanoporous PTMC thin films was studied *via* selective PDLLA etching, as presented in Figure 1.

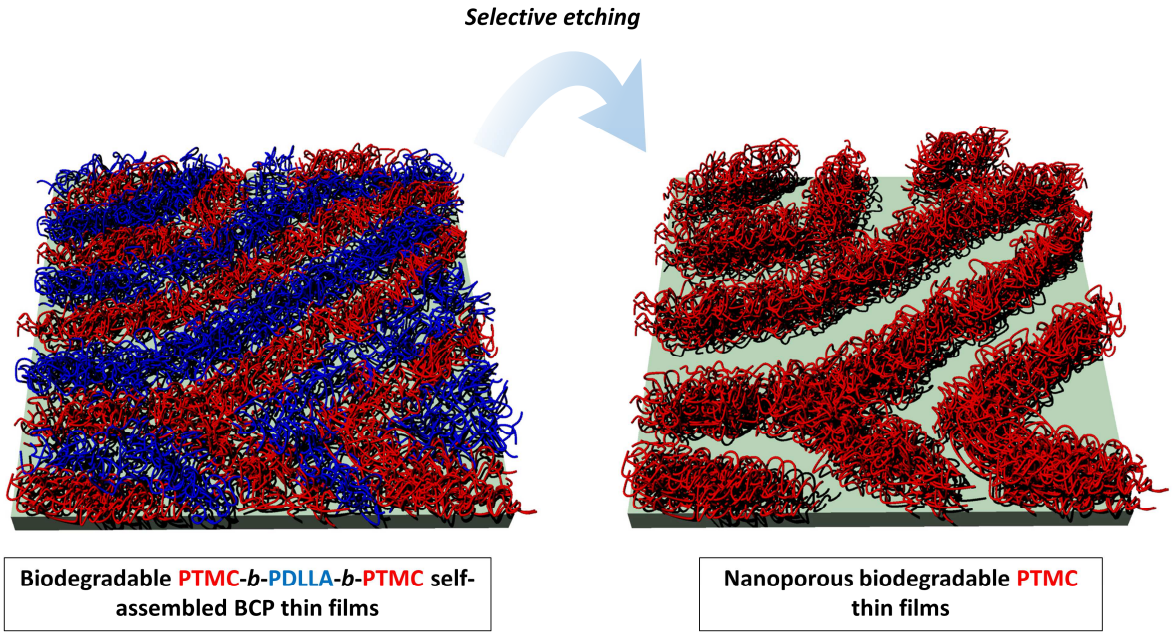

Figure 1. Graphical representation of the investigated PTMC-*b*-PDLLA-*b*-PTMC BCP thin films leading to nanoporous PTMC templates.

2. Experimental Section/Methods

Materials and chemicals

The DL-LA monomer was purchased from Corbion (The Netherlands), while TMC monomer was obtained from Foryou Medical (China). The catalyst (methanesulfonic acid (MSA)), initiator (1,6-hexane diol) and other chemicals such as methacrylic anhydride (MMA) and triethyl amine (TEA), as well as the solvents (chloroform, dichloromethane and propylene carbonate) were obtained from Sigma Aldrich (France) and used as received. Anhydrous dichloromethane, retrieved from solvent purificator Inert PureSolv™ (France), was employed as diluting medium for the triblock copolymer synthesis and their end-functionalization. 2-hydroxy-2-methylpropiophenone (Darocur 1173) was obtained from BASF Chemicals (Germany). Si-wafer

substrates ((100)-oriented, p-type/boron doped) were obtained from STMicroelectronics Co (Switzerland).

Synthesis of PTMC-b-PDLLA-b-PTMC triblock copolymer

The synthesis of the block copolymers employed in this study was previously reported.[23] Typically, in the case of the PTMC-*b*-PDLLA-*b*-PTMC block copolymer synthesis with defined molar ratios of PTMC/PDLLA = 50/50, the PDLLA macroinitiator (1,05 g, 0,138 mmol, 1 equiv.) was introduced in a round bottom flask with the TMC monomer (1,43 g, 13,8 mmol, 100 equiv.). Some vacuum-dry argon cycles were performed before the injection of the anhydrous dichloromethane solvent ($[TMC/PDLLA]_0$ = 1 mol/L). Finally, the MSA catalyst (0,026g, 0,276 mmol, 2 equiv.) was added to the reaction mixture. The reaction was performed at 30°C. After full TMC conversion as evidenced by NMR, an excess amount of triethylamine (3 equiv. in respect to catalyst) was added when using MSA, to neutralize this one. Finally, the polymers were slowly poured in cold methanol, then filtered and washed several times with methanol and dried in a vacuum oven for 24 h.

Synthesis of PTMC-b-PDLLA-b-PTMC dimethacrylates

Both $PTMC_{50}$-*b*-$PDLLA_{100}$-*b*-$PTMC_{50}$ and $PTMC_{100}$-*b*-$PDLLA_{100}$-*b*-$PTMC_{100}$ triblock copolymers (1,5 g, 1 equiv.) were methacrylated employing methacrylic anhydride (MMA) (0,053 g, 4 equiv.) with triethyl amine (TEA) (0,035 g, 4 equiv.) in anhydrous dichloromethane solution ($[triblock\ copolymer]_0$ = 0,2 $g.ml^{-1}$). The reaction was left stirring at room temperature in the dark for one week. Afterwards, the dimethacrylated copolymers were purified by precipitation in cold methanol, dried in vacuum oven at room temperature for 24 h and stored at -18°C until further use.

Polymer blend preparation

The homopolymer blends of PTMC and PDLLA (with 60/40 and 75/25 v/v ratios, respectively) were prepared by dissolving them in dicholoromethane (2 ml for 1g of polymer blend), followed by 24 h stirring. The blend was firstly separated by evaporation of the solvent, then dried under vacuum for 24 h.

Polymer characterizations

Nuclear magnetic resonance (NMR)

^{1}H NMR spectra were recorded a 400 MHz Bruker Aspect Spectrometer with $CDCl_3$ as deuterated solvent. Chemical shifts were defined in parts per million (ppm), whereas the reference peak was residual $CDCl_3$ at 7.26 ppm.

Differential scanning calorimetry (DSC)

DSC analyses were carried out on a Mettler Toledo (Mettler Toledo, France) DSC1 calorimeter, where constant calibrations were achieved using biphenyl, indium, bismium, zinc and cesium chloride standards. 12 to 15 mg of the samples (homopolymers, blends and triblock copolymers) were subjected to thermal analysis after purification and drying. The samples were heated from -150°C and 100°C with a heating of rate of 20°C/min and two cycles were recorded. Glass transition temperature (T_g) points were evaluated in the second scan of DSC thermograms, as the transition midpoint.

Thin film preparation

Spin-coating technique

Si-wafers were used as substrates for the spin-coating of thin films. The latter were prepared by spin-coating 10 µl of the blend or triblock copolymers solution at 10 wt % (in dichloromethane or propylene carbonate) at 4000 rpm during 90 s at room temperature. Films with thickness of 120 µm were obtained.

Photo-crosslinked thin films

In the case of photo-crosslinked films, prior to spin-coating, 5 wt % of photoinitiator (Darocur 1173) in respect to the polymer was added to the solution formulation for thin films. The photo-crosslinking (induced after solvent evaporation or solvent vapor annealing processes) was performed in a UV Crosslinker Biolink chamber (Thermo Fischer, France). The irradiation time was 10 min at 3 $mW.cm^{-2}$ using a 365 nm wavelength at 10 cm from the surface of the specimens. Disk samples with 1 cm of diameter and 2 mm thick were prepared to determine the photo-crosslinking efficiency of the block copolymers. For that, the gel content in dichloromethane as the selected solvent, was calculated following the Equation (1), where m_d is the mass of the dry samples after one extraction in dichloromethane and m_i is the initial mass of the dried samples just after photo-crosslinking.

$$\text{Gel content} = \frac{md}{mi} * 100 \quad (1)$$

Solvent evaporation

Once spin-coated, the thin films were placed in a chamber with controlled room temperature of 20°C for six hours under open air atmosphere. Afterwards, they were dried under vacuum at room temperature for 12 h.

Solvent-vapor annealing (SVA) of thin films

During the SVA process, the thin films from propylene carbonate solutions were exposed to vapors of the selected solvent (chloroform). The polymer solvent incompatibility ($\chi_{P\text{-}S}$) was calculated by Equation (2), where $V_{M,S}$ is the molar volume of the solvent, while δ_d is the dispersive and δ_p is the polar component of the polymer and the solvent.

$$\chi_{P-S} = \frac{\nu_{M,S}}{RT}\left((\delta_{P,d} - \delta_{S,d})^2 x (\delta_{P,p} - \delta_{S,p})^2\right) \quad (2)$$

Afterwards, the samples were placed in a closed desiccator of 4 L at 20°C. A constant solvent vapor pressure in the closed chamber was maintained thanks to a 40 mL of solvent in a beaker. The samples were placed on a support near the upper part of the desiccator while the solvent beaker was located on the bottom of the desiccator, to achieve the saturated solvent pressure. At the end of the SVA process (1 h or more), the thin films were removed from the desiccator and dried in vacuum oven at room temperature for 12 h.

Thermal treatment of thin films

For the samples thermally inspected after spin-coating and SVA, the thin-films were stored in a vacuum oven at 65°C for a specific time duration.

PDLLA-hydrolysis

Selective PDLLA etching from the self-assembled thin films was performed by covering the film surface with 0.5 M sodium hydroxide 40/60 (v/v) methanol/water solution for 30 min. After removal of the 0.5 M NaOH solution, the sample was washed with 40/60 (v/v) methanol/water solution for 10 min, before being dried under vacuum at room temperature for 24 h.

Thin film analysis

Atomic Force Microscopy (AFM)

The AFM mechanical characterization performed in HarmoniX mode from Bruker AFM is presented herein. Harmonix™ mode provides simultaneous topography and (semi)-quantitative mechanical property mapping at typical tapping mode imaging speed.[24] The relatively high bandwidth and force sensitivity of the so-called Torsional harmonic cantilever (THC) probes offers a good mechanical property in the mapping capability, especially for complex systems composed of different phases with contrasting properties.

THC soft probers (HMSX from Bruker) with spring constant of 0.5 to 1.5 $N.m^{-1}$ were used on a Nanoman V AFM from Bruker Instruments to record images at different magnifications (20x20 µm², 10x10 µm², 5x5 µm², 2x2 µm²) on different areas of the surface of each sample. The image resolution was 512 x 512 pixels with a scan rate of 0.5 Hz. The tapping ratio (the ratio of the setpoint amplitude to the free vibration amplitude, $r_{sp} = A_{sp}/A_0$) was set to 0.6 in order to maintain « hard tapping » conditions and to enhance the mechanical contrast on different materials while keeping a good spatial resolution. Several images at several magnifications were captured with the aim of improving the confidence in the statistical analysis. The DMT modulus sensitivity was calibrated by using a reference sample from Bruker Instruments (PS/LDPE) with

known modulus value (2.3 GPa/70 MPa). Our relative DMT modulus calibration gives 2.37 GPa ± 0.24 GPa and 73 MPa ± 9 MPa for PS and LDPE respectively.

Scanning electron microscopy (SEM)

The sample was firstly coated with an ultrathin layer of electrically conducting platinum that was deposited by high-vacuum evaporation. Afterwards, prior to analysis, it was folded on a 45° SEM mount. SEM experimentations were performed on Hitachi S-4800 instrument operating at a spatial resolution of 1.5 nm at 2 kV energy.

Transmission electron microscopy (TEM)

Transmission Electron Microscopy (TEM) was performed on a JEOL 1400Plus operated at 80 kV (Tungsten filament). TEM images were recorded with a high sensitivity sCMOS JEOL Matataki Flash 2048×2048 pixels². To avoid long electron beam exposition, all microscope and beam tunings were proceeded on a sacrificial part, and images were obtained on virgin sample part with the minimum electron dose from SYSTEM IN FRONTIER INC. The polymer samples for TEM analysis were prepared by embedding the film in LR White resin, the polymerization was done at -20°C after adding an accelerator. Embedded samples were cut with an ultramicrotome Leica UC7, ultrathin sections (70nm) were collected on 300 mesh carbon coated copper grids.

Small Angle X-ray Scattering (SAXS)

SAXS experiments were run using a homemade instrument using copolymer film coated on mylar, whose contribution was then subtracted from the acquired data.

Image analysis

AFM and TEM images were analysed using ImageJ software. Surface ratio of each phase were measured on processed binarized images. The average sizes of PDLLA domains were measured on at least 80 different locations and the standard deviations were reported.

3. Results and discussion

3.1 Theoretical considerations on the phase-separation in PTMC-*b*-PDLLA-*b*-PTMC triblock copolymers

In the direction of anticipating the possible phase-separation in a PTMC-PDLLA system, at first the Flory-Huggins PTMC-PDLLA ($\chi_{PTMC\text{-}PDLLA}$) interaction component was theoretically determined. This parameter measures the total interaction energy between a pair of polymer chains, in our case PTMC and PDLLA, and is defined by the following equation (3):

$$\chi_{AB} = \frac{\nu_{M,AB}}{RT}(\delta_A - \delta_B)^2 \quad (3)$$

$$\nu_M = \frac{M}{\rho_A} \quad (4)$$

where $\nu_{M,AB}$ is the geometric mean of the molar volumes of both polymers (calculated by equation (4) where ρ and M are the amorphous material density and molecular weight of the repeating unit), R and T are the universal gas constant and the absolute temperature, while $(\delta_A - \delta_B)^2$ is the cohesive energy density from the solubility parameters of both polymers (δ_{PTMC} and δ_{PDLLA}).

The Hoftyzer-van Krevelen method was used to calculate the solubility parameters for both PTMC and PDLLA leading to the Flory-Huggins interaction parameter (equations (5) to (8)):

$$\delta_T = \sqrt{\delta_d^2 + \delta_p^2 + \delta_h^2} \quad (5)$$

$$\delta_d = \frac{\Sigma F_{di}}{V_m} \quad (6)$$

$$\delta_p = \frac{\sqrt{\Sigma F_{pi}^2}}{V_m} \quad (7)$$

$$\delta_h = \frac{\sqrt{\Sigma E_{hi}}}{V_m} \quad (8)$$

This qualitative method is based on the determination of the solubility parameters by the group-contribution approach. The latter is an approximation applying the additivity rule of contributions of the structural and functional groups of the repeating unit in a polymer chain. In fact, the Hoftyzer-van Krevelen method, among others such as Hansen's or Hoy's ones, is the most suitable for amorphous polymers, since they particularly optimized the group contributions from experimental data for numerous non-crystalline polymers.[25] Therefore, the solubility parameter ($\delta_{T,polymer}$) is calculated as represented in equation (4), and is in direct dependence on the dispersion (δ_d), the polarity (δ_p) and the hydrogen bonding (δ_h) components. Therein, F_{di}, F_{pi} are group contributions while E_{hi}, also calculated by the group-contribution approach stands for the hydrogen bonding energy. On the other side, V_m means the molar volume of the polymer repeating unit.

Accordingly, by using the contributions of each group present in the repeating unit of a respective polymer, the values of the group-contribution segments (F_{di}, F_{pi} and E_{hi}) for both PTMC and PDLLA were firstly calculated. The results are depicted in table (1A) and table (1B), respectively.

Table 1A. Determination of the solubility parameter component group contributions of PTMC with a repeating unit [-O-CH_2-CH_2-CH_2-O-CO-].

Chemical groups	$\mathbf{F_{di}}$	$\mathbf{F_{pi}^2}$	$\mathbf{E_{hi}}$
-O-	100	160 000	3000
3 -CH_2-	810	0	0
-O-CO-	390	240100	7000
Σ	1300	400100	10 000

Table 1B. Determination of the solubility parameter component group contributions of PDLLA with a repeating unit [-O-CH(CH_3)-CO-].

Chemical groups	$\mathbf{F_{di}}$	$\mathbf{F_{pi}^2}$	$\mathbf{E_{hi}}$
-CH-	80	0	0
-CH_3-	420	0	0
-O-CO-	390	240100	7000
Σ	890	240100	7000

By applying these values in the equations (6) to (8), and consequently by using the equation (5), the overall values of PTMC and PDLLA solubility parameters were determined, as presented in Table 2.

Table 2. PTMC and PDLLA solubility parameters (δ_T) and their dispersion, polar and hydrogen bonding component.

Polymers	δ_T $(MPa)^{0.5}$	δ_d $(MPa)^{0.5}$	δ_p $(MPa)^{0.5}$	δ_h $(MPa)^{0.5}$	V_m $(ml.mol^{-1})$
Poly (D,L-lactic acid)	18.2	13.2	7.3	10.2	67.2
Poly (trimethylenecarbonate)	21.7	16.7	8.1	11.3	78

Therefore, by implementing the equation (3) when using δ_A as solubility parameter for PTMC and δ_B as solubility parameter for PDLLA, the PTMC-PDLLA interaction parameter gives a value of 0.36 (Table 3). The segregation trend of the system can be predicted since it can be measured by the $\chi_{AB}N$ product term. N stands for the number of repeating units of both blocks. In our study, the number of repeating units of the PDLLA middle-block was settled to 100, while the PTMC end-blocks had 100 and 200 repeating units (Table 3). The volume fraction of the blocks was determined by Equation (9), taking into consideration that $f_{PTMC} + f_{PDLLA} = 1$.

$$f_{PTMC} = \frac{(M_{w,PTMC} \times d_{PTMC})}{(M_{w,PTMC} \times d_{PTMC}) + (M_{w,PDLLA} \times d_{PDLLA})} \quad (9)$$

Where d_{PTMC} = 1.316 $g.cm^{-3}$ and d_{PLA} = 1.161 $g.cm^{-3}$ are the density values of the respective PTMC and PDLLA amorphous polymers.

The defined block lengths of PTMC and PDLLA were set on purpose for the synthesis of the *t*BCPs employed in this study, so that the system could belong to the strong segregational limit (χN >> 10.5).[26] This parameter is crucial in the aim of satisfying the theoretical requirements for phase-separation in a blend or in a copolymer system.

Table 3. $\chi_{AB}N$ values for PTMC-PDLLA block copolymers as a function of their respective volume fractions and Flory-Huggins interaction parameter.

Block copolymer	**block molar ratio**	**block volume fractions**	**Calculated $\chi_{PTMC-PDLLA}$**	**$\chi_{AB}N$ value**
$PTMC_{50}$-*b*-$PDLLA_{100}$-*b*-$PTMC_{50}$	50/50	60/40	0.36	72
$PTMC_{100}$-*b*-$PDLLA_{100}$-*b*-$PTMC_{100}$	67/33	75/25	0.36	108

3.2 End-functionalization of PTMC-*b*-PDLLA-*b*-PTMC dimethacrylate (*dMa*) triblock copolymers.

Formerly reported literature data pointed out towards challenging synthesis of block copolymers employing PDLLA macroinitiators (later used as the middle block) due to the partial reactivity of secondary hydroxyl chain ends. Nevertheless, we managed to surpass this problem by employing a specific organocatalytic system following an activated monomer mechanism for the ring-opening polymerization of TMC from PDLLA macroinitiators, as reported in our previous study.[23] Hence, in that publication we demonstrated the controlled synthesis of the PTMC-*b*-PDLLA-*b*-PTMC triblock copolymers. In Figure 2, NMR investigations are displayed together with the synthetic procedure, where ^{1}H NMR justified the desired block proportions, ^{13}C NMR implicated the absence of any side reactions such as transesterification, while NMR-DOSY

confirmed the absence of side products such as PDLLA homopolymer. In addition, both SEC chromatograms show monomodal peaks that shifted from the PDLLA macroinitiator one (Figure S1 (Figure S1).

Hence, two types of PTMC-*b*-PDLLA-*b*-PTMC triblock copolymers were investigated in this study. The NMR spectroscopy was used to determine the composition of both studied copolymers. For the triblock PTMC/PDLLA molar ratio of 50/50, a total molar mass of 17.4 $kg.mol^{-1}$ with Mn (PDLLA) = 7.2 $kg.mol^{-1}$ and M_n (PTMC) = 10.2 $kg.mol^{-1}$ was calculated, while the triblock copolymer PTMC/PDLLA with molar ratio of 67/33 displayed a total molar mass of 27.8 $kg.mol^{-1}$ with M_n (PTMC) = 20.6 $kg.mol^{-1}$ and M_n (PDLLA) = 7.2 $kg.mol^{-1}$. The dispersities Đ, obtained by SEC, were 1.23 and 1.27, respectively. The integrity of the SEC data of the respective homopolymers and the herein employed triblock copolymers is reported in the previous investigation.[23]

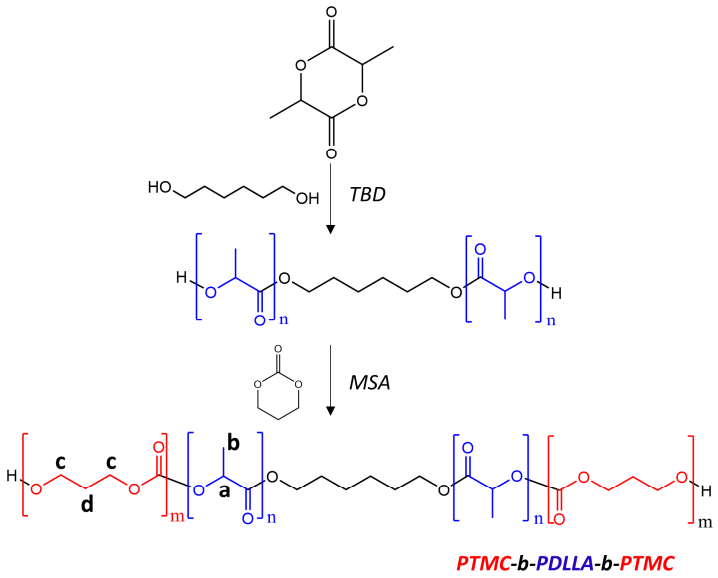

PTMC-b-PDLLA-b-PTMC

^{13}C-NMR

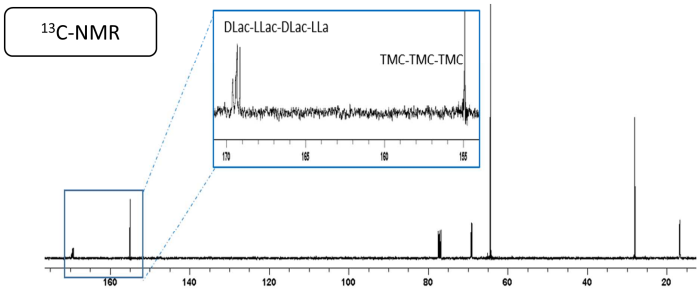

NMR-DOSY

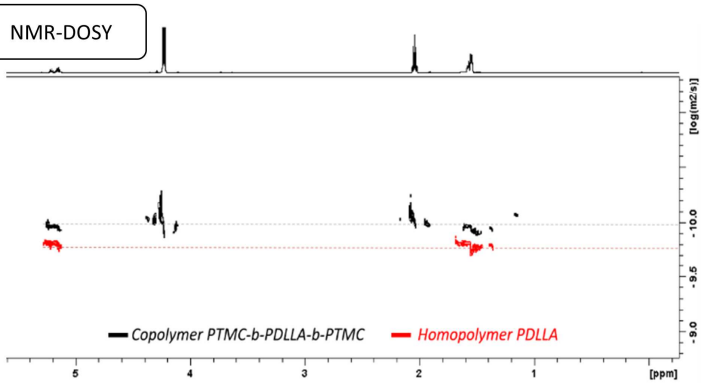

^{1}H-NMR

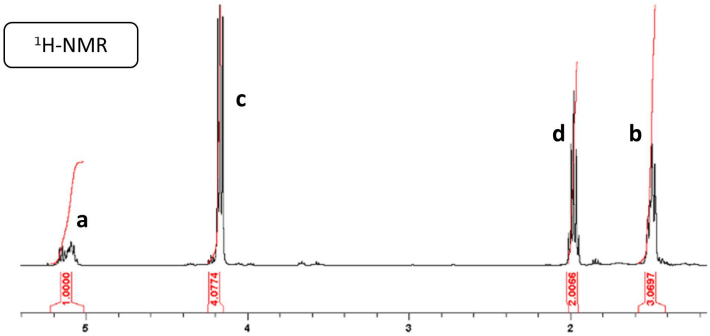

Figure 2. The synthesis procedure, ^{13}C-NMR, NMR-DOSY and ^{1}H NMR spectra of the PTMC$_{50}$-*b*-PDLLA$_{100}$-*b*-PTMC$_{50}$ triblock copolymer.

An ultimate modification of the block copolymers was performed before proceeding to the investigation of the self-assembly in the PTMC/PDLLA system. Therefore, in the goal of the (porous) matrix stabilization, end-functionalization of the BCPs with methacrylate groups was performed (Figure 3), the latter having the ability to lead to photo-crosslinked thin films under UV light and in the presence of photo-initiator. In Figure S2, ^{1}H NMR spectrum of dimethacrylated PTMC-*b*-PDLLA-*b*-PTMC is presented. The elevated functionalization percentage (≈ 87 %) is calculated as presented in equation (10).

$$Functionalisation\ \% = \frac{\int_{5.56ppm}^{5.52ppm} H_a + \int_{6.09ppm}^{6.085ppm} H_b \Big/ 4}{\int_{5.21ppm}^{5.02ppm} CH_{(PDLLA)} \Big/ 100} \quad (10)$$

Hence, the result is obtained by comparing the characteristic peaks of the double bond methacrylate units (integration of the protons situated at 5.5 and 6.1 ppm) with the peaks of the CH protons belonging to the middle PDLLA block in the copolymer structure.

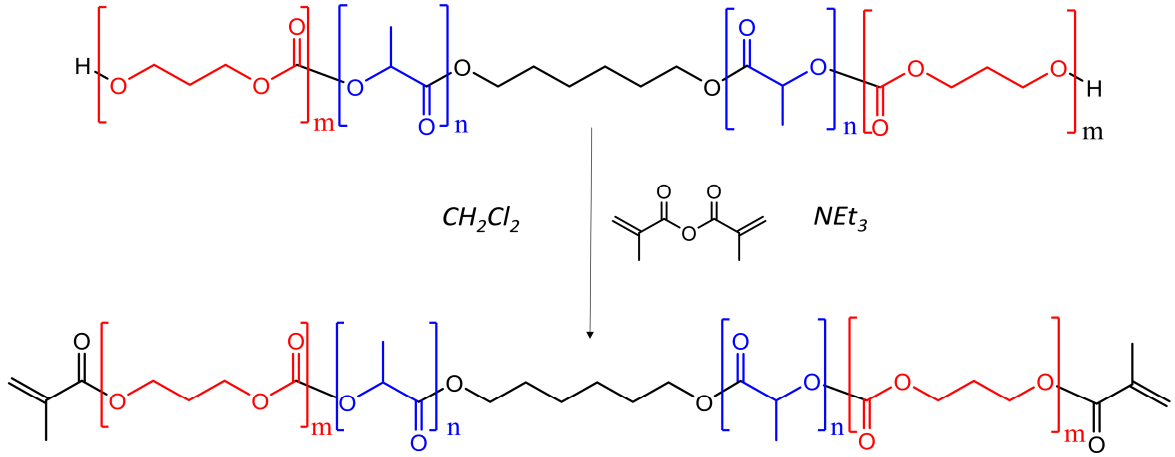

Figure 3. PTMC-*b*-PDLLA-*b*-PTMC triblock copolymers functionalization with photo-sensitive methacrylate end-groups.

Finally, photosensitive block copolymers were spin-coated and photo-crosslinked in presence of photo-initiator and UV irradiation. The gel content in dichloromethane as solvent approximated values of around 92 %, showing the efficiency of the photo-crosslinking step. Moreover, this curing process increased the film robustness and its mechanical resistance.

3.3 Phase-separation and self-assembly phenomena in PTMC/PDLLA blends, triblock copolymers, and photo-crosslinked triblock copolymers

3.3.1 Differential scanning calorimetry (DSC) as a tool for studying phase-separation

DSC technique has been widely used to access the thermal properties of composites, polymer blends and self-organized associations.[27, 28] Moreover, the observable glass transition

temperature is directly related to the phase equilibrium and the miscibility character of a polymer system. Hence, if a single broad glass transition scope is observed, a polymer blend can be considered as miscible. On the contrary, immiscible structures precisely demonstrate two distinct Tg points.

Therefore, DSC scans of PTMC$_{50}$-*b*-PDLLA$_{100}$-*b*-PTMC$_{50}$ and PTMC$_{100}$-*b*-PDLLA$_{100}$-*b*-PTMC$_{100}$ triblock copolymers were performed, and their respective glass transitions were compared to the ones of PTMC and PDLLA homopolymers. The thermograms of the *t*BCPs can be visualized in Figure 4.

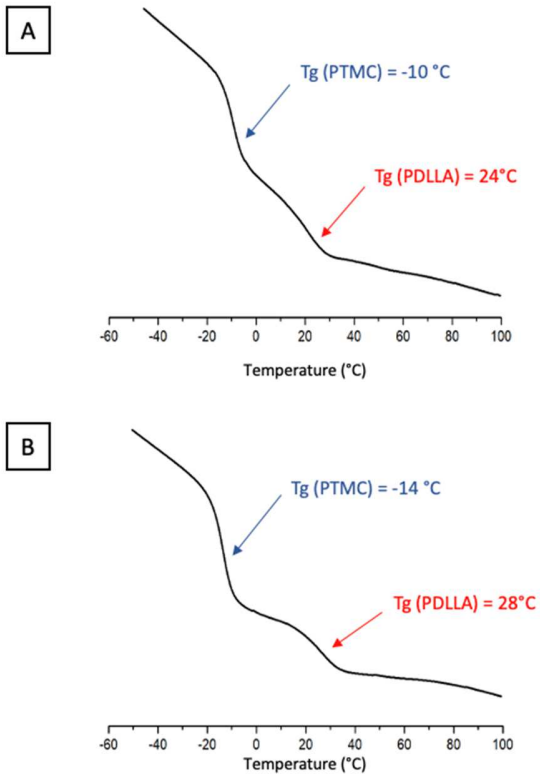

Figure 4. DSC cooling scans of PTMC$_{50}$-*b*-PDLLA$_{100}$-*b*-PTMC$_{50}$ (A) and PTMC$_{100}$-*b*-PDLLA$_{100}$-*b*-PTMC$_{100}$ (B).

The phase-separation in PTMC-*b*-PDLLA-*b*-PTMC triblock copolymers (with differing molar ratios) was confirmed with the appearance of two glass transition temperatures, close to that of the corresponding homopolymers (Table 4). This behavior is in accordance with the previously discussed thermodynamic data of Table 3.

Table 4. Values of glass transition temperatures of the homopolymers and triblock copolymers.

Samples	Tg (PTMC) (°C)	Tg (PDLLA) (°C)
$PTMC_{100}$	-17	/
$PDLLA_{100}$	/	27
$PTMC_{50}$-*b*-$PDLLA_{100}$-*b*-$PTMC_{50}$ *t*BCP	-10	24
$PTMC_{100}$-*b*-$PDLLA_{100}$-*b*-$PTMC_{100}$ *t*BCP	-14	28

Since the thermal analysis of the triblock copolymers points out a phase-separated system, we continued the investigation of the block copolymer self-assembly on thin films.

3.3.2. Film preparation based on PTMC/PDLLA systems

Two major obstacles persist when aiming for defect-free nanoporous structures: i/ achieving long-range order upon BCP self-assembly, and ii/ etching conditions preserving the matrix integrity and its mechanical properties.[29-31] Therefore, the most used methods for enhancing long-range order in BCPs systems are either thermal or solvent vapor annealing, known to induce additional mobility to the polymer chains to achieve the least energetically demanding morphology.[32, 33] On the other side, matrix crosslinking has been often used as an advantageous method to strengthened both mechanical properties and robustness of the porous component.[34] Multiple parameters such as the type of material (blend or block copolymer), the

influence of the copolymer composition together with photo-crosslinking, the annealing techniques such as solvent vapor annealing (SVA) or the choice of the SVA solvent have been inspected to optimize the self-assembly conditions of the PTMC/PDLLA system. Finally, a special interest was dedicated to the impact on triblock copolymer phase organization upon photo-crosslinking treatment.

3.3.3. Study of the PTMC-b-PDLLA-b-PTMC block copolymer phase-separation by Atomic Force Microscopy (AFM)

The phase separation phenomena taking place in solid state thin films of blends or block copolymers have been more and more investigated by AFM since the latter gives the opportunity to characterize differing nanoscale processes occurring at the top-surface of materials. By measuring the pressure variations between the sample surface and the AFM tip, a cartography of the microdomains together with their properties such as size, shape, organization into various morphologies but also an insight in their elasticity is provided.[35] Among the three AFM operation modes, the tapping mode offers an optimal imaging resolution. Meanwhile, due to the remarkably short interval of tip-surface contact, the distortion of surface topography, occasionally occurring when analyzing elastomers in contact mode is avoided. Moreover, the elastic moduli of PTMC (≈ 6 MPa) and PDLLA (≈ 4 GPa) being significantly contrasted, favors the AFM characterization. By these means, tapping-mode AFM was chosen for investigating the phase-separation morphologies of all the systems PTMC/PDLLA.

Solvent evaporation method

In the first place, as the most straightforward approach, a simple solvent evaporation from thin films has been examined on the blends and the triblock copolymers. Thus, the samples were primarily processed in a thin film geometry *via* spin-coating and further quenched by fast solvent evaporation at room temperature. This elementary process is known to produce ordered microdomain morphologies in BCP thin films,[36] where the latter is a result of an ordering front in the thin film propagating from the surface to its interior as the solvent evaporates.[37]

For that purpose, a good solvent for both PTMC and PDLLA components with low boiling temperature was chosen as the diluting medium for spin-coating. Therefore, dichloromethane appeared to be the fitting candidate for such requirement. Hence, once this solvent was evaporated, the dried films were analyzed by AFM.

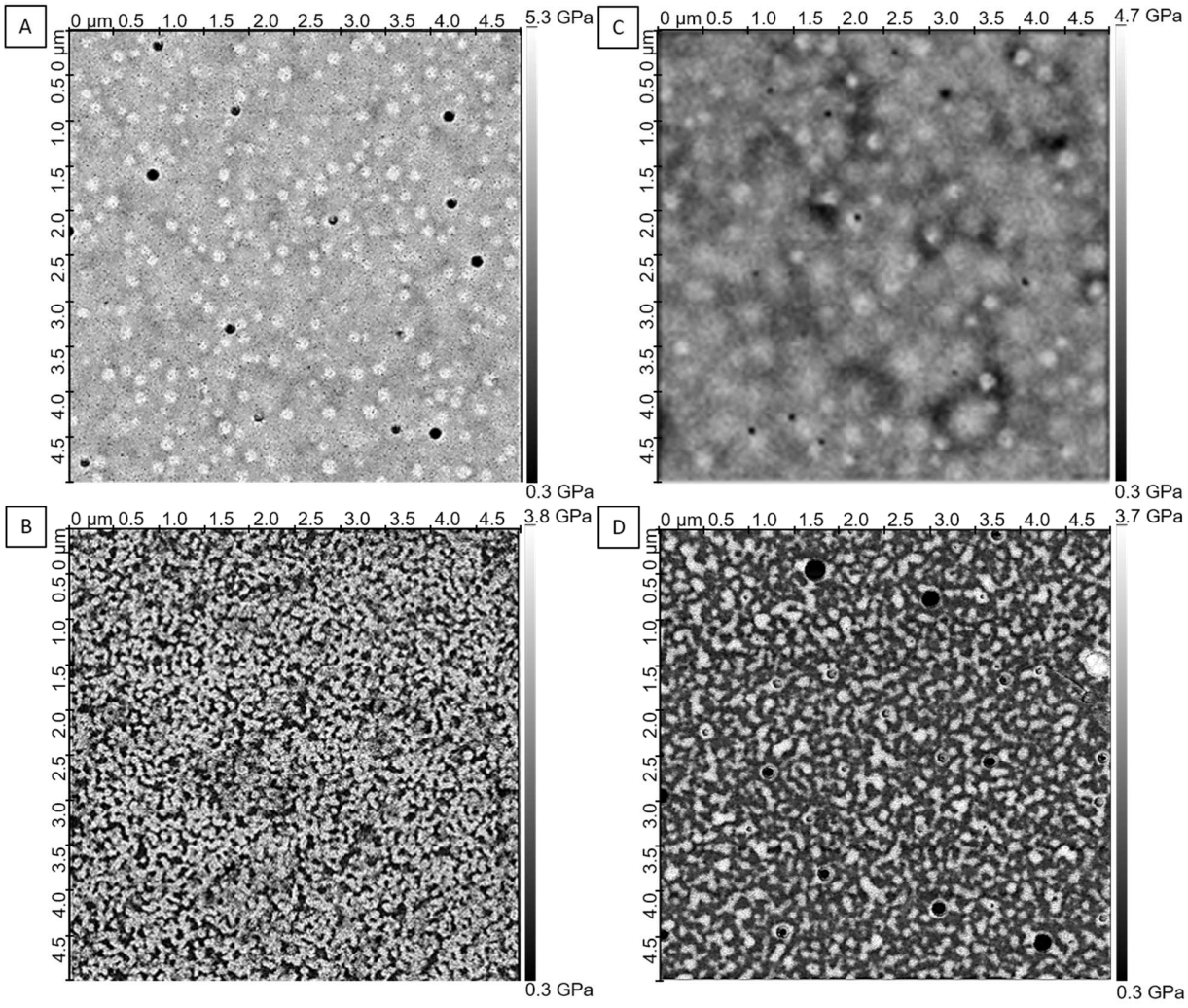

Figure 5. AFM stiffness images of thin films A) $PTMC_{100}$/$PDLLA_{100}$ blend, B) $PTMC_{50}$-*b*-$PDLLA_{100}$-*b*-$PTMC_{50}$, C) $PTMC_{200}$/$PDLLA_{100}$ blend and D) $PTMC_{100}$-*b*-$PDLLA_{100}$-*b*-$PTMC_{100}$ *t*BCP on 5 x 5µm length scale. The white areas correspond to PDLLA (high modulus); the dark areas correspond to PTMC (low modulus).

Figure 5 displays AFM stiffness images of spin-coated PTMC/PDLLA blends and copolymer thin films, with two varied volume ratios between the components. In this kinetically trapped self-assembly, the PDLLA phase appears bright due to its rigidity with a Young modulus magnitude of around 4 GPa close to the values reported in the literature,[38] while the rubber-

like PTMC phase occurs darker with magnitudes of around 0.3 GPa. However, even though the contrast appears obvious, the value for PTMC phase remains widely above the modulus of typical elastomeric PTMC around 6 MPa,[39] which is due to the detection limitation of the AFM tip that gives an overestimated value.

From these images, an evident difference is observable between the blend samples and the ones of $PTMC_{50}$-*b*-$PDLLA_{100}$-*b*-$PTMC_{50}$ and $PTMC_{100}$-*b*-$PDLLA_{100}$-*b*-$PTMC_{100}$ *t*BCPs. On one side, the blend demonstrates a smooth surface of almost homogeneous polymer layer with islands consisting of the PDLLA phase. On the other side, for the triblock copolymer architecture, even though highly ordered morphologies were not discernible, bicontinuous phase-separation on the nanometer range scale is clearly present.

Image J software calculations on the $PTMC_{50}$-*b*-$PDLLA_{100}$-*b*-$PTMC_{50}$ BCP thin film represented in the Figure 5B point toward 70 nm domain size of the PDLLA phase and PDLLA/PTMC respective surface ratio of 53/47 % on the analyzed surface, which is relatively close to the initial proportions between both blocks (Table 5). Likewise, the calculations on the $PTMC_{100}$-*b*-$PDLLA_{100}$-*b*-$PTMC_{100}$ BCP thin film presented in Figure 5D demonstrate a PDLLA domain size of 100 nm and PTMC/PDLLA respective ratio of 70/30 %. PDLLA domain size calculations are important since the latter represent the sacrificial block and could possibly lead to an initial idea of the size of the generated pores. In addition, as observable in both Table 5 and Figure 5, the higher proportion of PTMC in the triblock copolymer is in accordance with the AFM images where a higher proportion of the black PTMC region is clearly visible compared to the presence of white PDLLA area.

Table 5. Calculation of the PDLLA domain sizes and the PTMC surface ratio for the non-cured PTMC$_{\mathbf{50}}$-*b*-PDLLA$_{100}$-*b*-PTMC$_{\mathbf{50}}$ and PTMC$_{\mathbf{100}}$-*b*-PDLLA$_{100}$-*b*-PTMC$_{\mathbf{100}}$ thin films obtained by the solvent evaporation method.

Block copolymer	Treatment	%PTMC	L_{PDLLA} (nm)[a]	σ (nm)[b]
PTMC$_{50}$-*b*-PDLLA$_{100}$-*b*-PTMC$_{50}$	Solvent evaporation	47 %	70	20
PTMC$_{100}$-*b*-PDLLA$_{100}$-*b*-PTMC$_{100}$	Solvent evaporation	70 %	100	20

[a] mean PDLLA domain size (n>80), [b] standard deviation

Nevertheless, even though phase-separated structures were observable in the *t*BCP architectures herein, these images show the early stage of self-assembly since the fast solvent evaporation kinetically traps the as-spun thin films in a disordered state. Hence, additional mobility of the polymer chains should be induced to achieve better organized morphologies. Therefore, we used solvent vapor annealing in the aim to achieve an optimized self-assembly in the PTMC-*b*-PDLLA-*b*-PTMC triblock copolymers.

Solvent vapor annealing (SVA) approach

Solvent vapor annealing is an advantageous technique allowing achievement of ordered morphologies and domains even in BCPs of high molar masses and elevated Flory-Huggins interaction parameters, as in this study. This method is known to lead to faster self-assembly reorganization compared to thermal annealing, attainable even in lower temperatures (such as room temperature in some cases) due to the favorable thermodynamic forces in the swollen state,

causing an optimized control of the phenomena occurring at the BCP interface.[40, 41] To the letter, the SVA approach consists in exposing the thin films to vapors of precisely selected solvent. By absorbing this solvent, the polymer swells, thus allowing bigger mobility of the polymer chains leading to metastable morphologies, unachievable by other approaches.[42, 43] Moreover, SVA is beneficial to PDLLA containing block copolymers due to its sensitivity to hydrolysis which can be enhanced by the temperature rise.[38]

In our study, both block copolymer compositions were tested for the SVA approach, with a precisely selected solvent, given the fact that the solvent choice for the swollen state is being highly important for well-controlled ordered morphologies.[44] Moreover, the solvent used for spin-coating plays a big role in the phase organization though the SVA approach. Therefore, we studied which solvent couple (diluent solvent and SVA solvent) would be the most optimal to generate a nanometric organized phase separation. Propylene carbonate (PC) was chosen as diluent medium for the preparation of thin films. PC is a good solvent for both blocks with an elevated evaporation point, which allows a convenient reorganization in the SVA state. Regarding the solvent for the SVA process, various possibilities have been investigated. On one hand, when THF or ethanol were used as SVA solvents, undesired self-assemblies were obtained (Figure S3). On the other side, the highest level or self-assembly organization was achieved by using the solvent couple PC/chloroform. Such occurrence could be explained by the good compatibility of both blocks with chloroform, but also by the slight selectivity of this solvent to one of the blocks (PTMC), which is strongly suggested for the SVA process and observable by our calculations of polymer-solvent compatibilities ($\chi_{PTMC\text{-}chloroform}=0.92$, $\chi_{PDLLA\text{-}chloroform}=1.26$, as calculated by the equation (2) from the experimental part).

Despite the promoting annealing conditions, once again, the blend sample did not undertake clear phase-separation (Figure 6A). On the other side, well-ordered morphologies for the $PTMC_{100}$-*b*-$PDLLA_{100}$-*b*-$PTMC_{100}$ *t*BCP with remarkable phase-organization on the entire film surface are clearly observable in Figure 6B. PDLLA mean domain size is in the range of 90 nm while the proportions between the PTMC and the PDLLA phase are of 65% and 35%, respectively (Table 6). Moreover, the uniformity, achieved under brief annealing times of 1 h, was kept on a long-length scale of 20 x 20 μm, much larger than numerous literature examples of reported self-assemblies.[37, 45, 46] This result could be expected taking into account that the optimal SVA assemblies come from good solvents for both blocks or preferential to one of the blocks.[33] Hence, it can be concluded that the SVA process further promoted the phase-organization when compared to simple solvent evaporation. The Young Modulus of both phases remained consistent as in the previous case.

To investigate the organization of the $PTMC_{100}$-*b*-$PDLLA_{100}$-*b*-$PTMC_{100}$ *t*BCP within the entire film, the sample was analyzed by small angle X-ray scattering (SAXS). The obtained curve shows a q^{-4} decay of the signal in the low-q region, which confirms the presence of heterogeneous self-assembly with sharp interfaces (Figure S4A). Moreover, a peak is observed at $q=0.078$ nm^{-1}, corresponding to a characteristic length of 81 nm (Figure S4B), the low relative intensity of the peak coming from the weak electronic contrast between the different polymer domains. This result further confirms the self-assembled organization of the BCP within the film, with an average distance between PDLLA and PTMC domains of 81 nm. Interestingly, this value is close to the size of PDLLA domains observed on AFM images (90 nm), suggesting that PDLLA and PTMC domains have similar sizes. Yet, it should be noticed that the peak is observed close to the q-range lower limit of the analysis device; an ultra small angle X-ray

scattering (USAXS) analysis may provide more information on the organization at these length scales.[47]

Phase separation of $PTMC_{50}$-*b*-$PDLLA_{100}$-*b*-$PTMC_{50}$ *t*BCP using SVA approach also resulted in self-assembled organization and is presented in Figure S5. In this AFM image, the PTMC phase occupied 52% of the analyzed surface, while the PDLLA phase 48%. The domain size of the latter one approached 80 nm (Table 6). However, it can be noticed that better morphologies, in the case of the SVA treatment and contrary to simple solvent evaporation, were achieved for the triblock copolymer containing the higher ratio of the PTMC component.

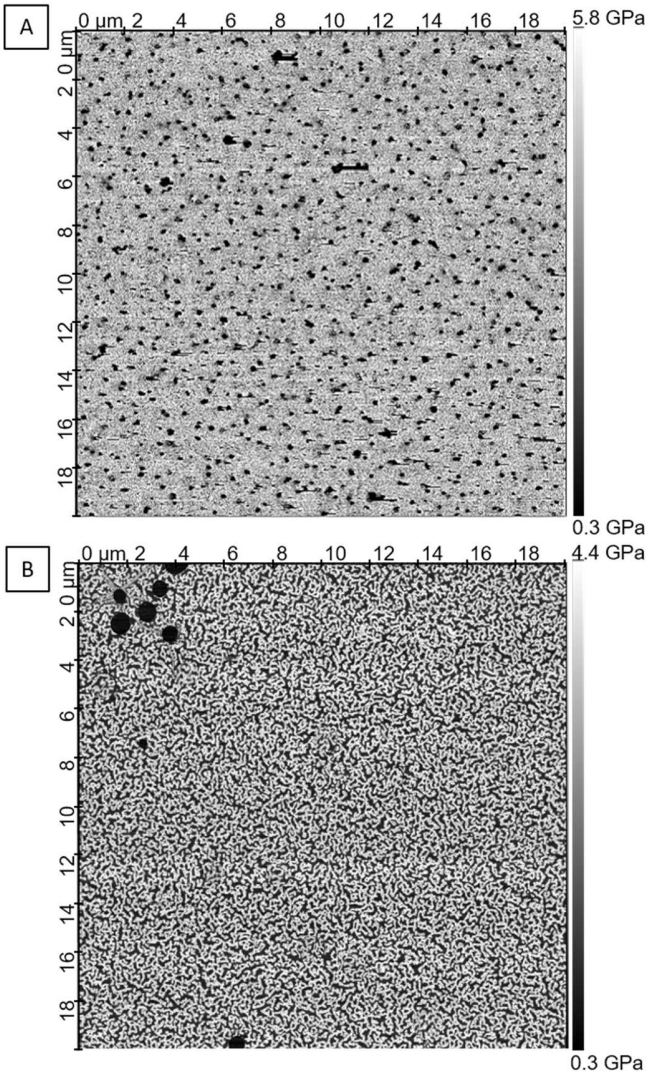

Figure 6. AFM stiffness images of solvent vapor annealed A) $PTMC_{200}$/$PDLLA_{100}$ blend; B) $PTMC_{100}$-*b*-$PDLLA_{100}$-*b*-$PTMC_{100}$ *t*BCP on 20 x 20 µm length scale. The white areas correspond to PDLLA (high modulus); the dark areas correspond to PTMC (low modulus).

Table 6. Calculation of the PDLLA domain sizes and the PTMC surface ratio for the non-cured $PTMC_{50}$-*b*-$PDLLA_{100}$-*b*-$PTMC_{50}$ and $PTMC_{100}$-*b*-$PDLLA_{100}$-*b*-$PTMC_{100}$ thin films obtained by the solvent vapor annealing method.

Block copolymer	Treatment	%PTMC	L_{PDLLA} (nm)[a]	σ (nm)[b]
$PTMC_{50}$-*b*-$PDLLA_{100}$-*b*-$PTMC_{50}$	SVA	52 %	80	20
$PTMC_{100}$-*b*-$PDLLA_{100}$-*b*-$PTMC_{100}$	SVA	65 %	90	20

[a] mean PDLLA domain size (n>80), [b] standard deviation

3.3.4. Photo-crosslinking impact on the PTMC-b-PDLLA-b-PTMC block copolymer phase-separation

Finally, the films were cured under UV irradiation to induce additional stability to the PTMC phase, presumed to support the cavities after PDLLA removal. In fact, polymer matrix crosslinking as a method for porous structure stabilization already showed benefits in various porous monoliths and thin films.[9] However, it is crucial to determine whether or not the photo-crosslinking treatment impacts the phase organization compared to that of the triblock copolymers. Consequently, both approaches of film preparation (the solvent evaporation and the SVA methods), were employed to explore the phase organization of dimethacrylated PTMC-*b*-PDLLA-*b*-PTMC followed by photo-crosslinking under UV irradiation. In addition, it must be noted that the photo-crosslinking was performed after the SVA process and film drying, so that no restriction of the chain mobility could occur.

Figure 7 represents AFM stiffness images of solvent evaporated and photo-crosslinked $PTMC_{50}$-*b*-$PDLLA_{100}$-*b*-$PTMC_{50}$ and $PTMC_{100}$-*b*-$PDLLA_{100}$-*b*-$PTMC_{100}$ *t*BCPs thin films. At initial sight, the phase organization is corresponding to that of the non-cured block copolymers obtained after simple solvent evaporation. Likewise, as presented in Table 7, the domain

proportions between the PTMC and PDLLA phase stay closely consistent as in the non-crosslinked samples. Therefore, even if a small increase of 40 nm in size of the PDLLA domains can be noticed for the cured $PTMC_{50}$-*b*-$PDLLA_{100}$-*b*-$PTMC_{50}$ *t*BCP compared to the non-cured counterpart, the photo-crosslinking did not disrupt the phase organization after simple solvent evaporation from the thin films. Nevertheless, more attractive is the observation of a bicontinuous morphology consisting of PTMC and PDLLA phases that remains highly remarkable on a large 20 x 20 µm length scale upon the combination of solvent vapor annealing and photo-crosslinking (Figure 8).

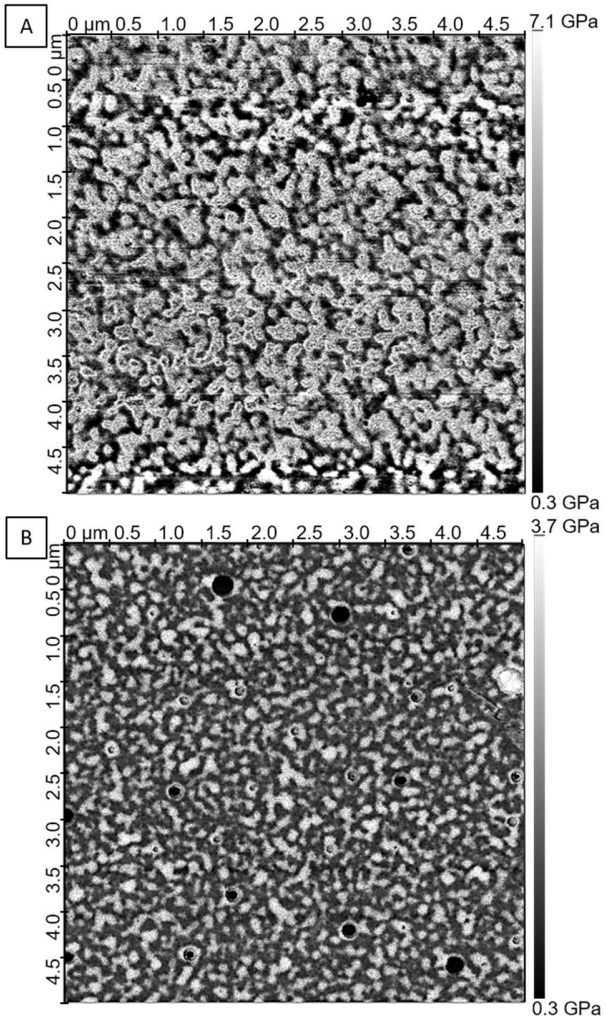

Figure 7. AFM stiffness images of solvent evaporated A) photo-crosslinked $PTMC_{50}$-*b*-$PDLLA_{100}$-*b*-$PTMC_{50}$ *t*BCP thin film on 5 x 5 μm length scale and B) photo-crosslinked $PTMC_{100}$-*b*-$PDLLA_{100}$-*b*-$PTMC_{100}$ *t*BCP thin film on 5 x 5 μm length scale. The white areas correspond to PDLLA (high modulus); the dark areas correspond to PTMC (low modulus).

Alike in the previous case of solvent evaporation and crosslinking, even though the block proportions remain consistent, we notice an increase in the sizes of the respective domains when employing SVA and crosslinking. As presented in Figure 8, by comparing the photo-crosslinked and solvent vapor annealed with the non-cured and solvent vapor annealed $PTMC_{100}$-*b*-$PDLLA_{100}$-*b*-$PTMC_{100}$ *t*BCP thin-film, an increase of 80 nm in the PDLLA domain size can be observed in the cured sample, which also leads to slightly higher surface detection of PDLLA domains (as compared from Table 6 and Table 7). Similarly, the domain size difference between the cured and non-cured $PTMC_{50}$-*b*-$PDLLA_{100}$-*b*-$PTMC_{50}$ is increased by 20 nm. This increase of PDLLA mean domain size with the photo-crosslinking may be due to the shrinkage of the PTMC phase, which would also explain the slight decrease of PTMC surface ratio. In fact, the occurring shrinkage could be quite expected since it is due to the contraction of the system usually taking place in cured environments. However, it can be concluded that the photo-crosslinking of methacrylated PTMC did not disrupt the overall self-assembly of the BCP association and preserved the phase-organization.

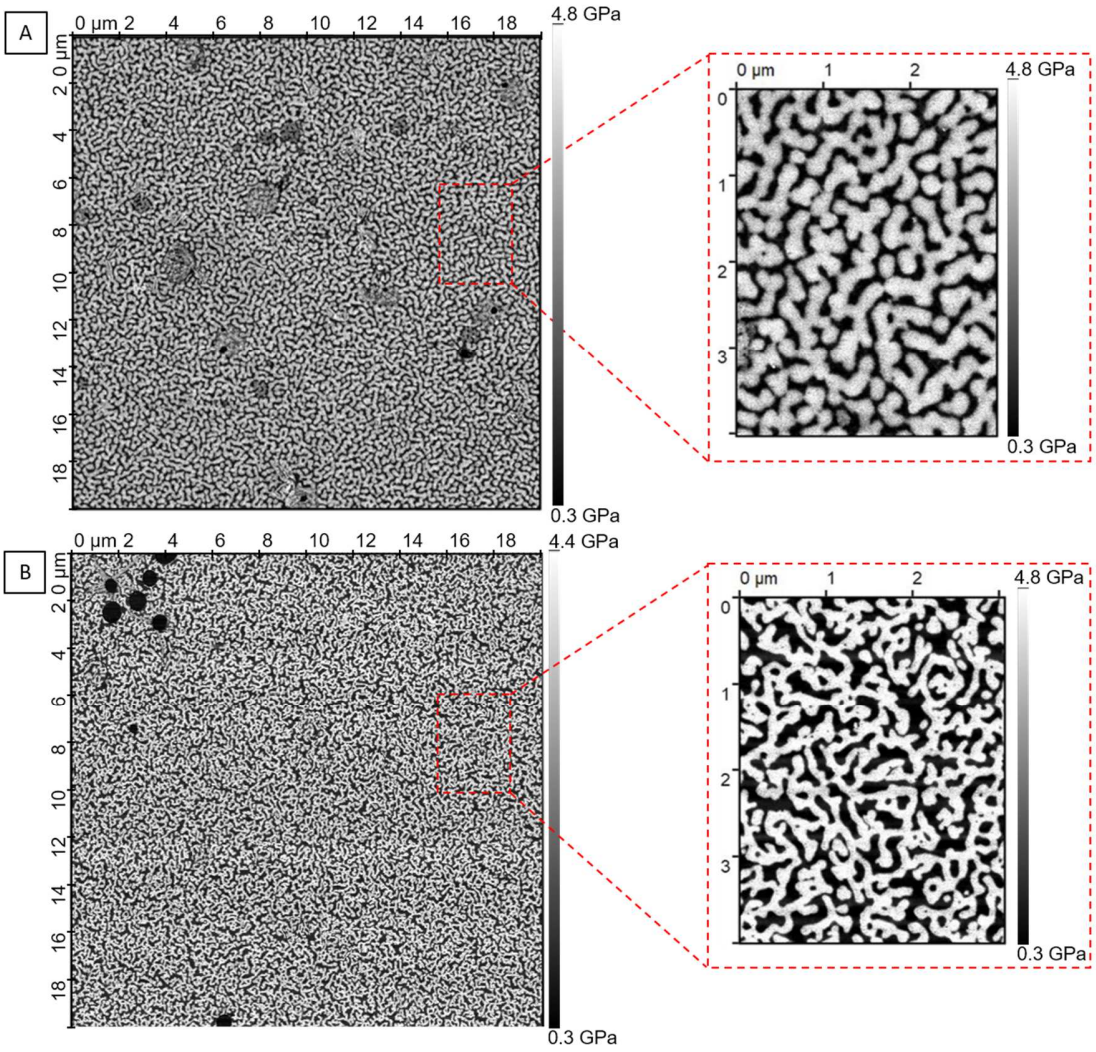

Figure 8. AFM stiffness images of solvent-vapor annealed: A) photo-crosslinked PTMC$_{100}$-*b*-PDLLA$_{100}$-*b*-PTMC$_{100}$ *t*BCP thin film on 5 x 5 µm length scale with a zoomed part with 4 x 3 µm length scale and B) non-photo-crosslinked PTMC$_{100}$-*b*-PDLLA$_{100}$-*b*-PTMC$_{100}$ *t*BCP thin film on 5 x 5 µm length scale with a zoomed part with 4 x 3 µm length scale. The white areas correspond to PDLLA (high modulus); the dark areas correspond to PTMC (low modulus).

Table 7. Calculation of the PDLLA domain sizes and the PTMC surface ratio for the crosslinked PTMC$_{50}$-*b*-PDLLA$_{100}$-*b*-PTMC$_{50}$ and PTMC$_{100}$-*b*-PDLLA$_{100}$-*b*-PTMC$_{100}$ thin films.

Block copolymer	Treatment	%PTMC	L_{PDLLA} (nm)[a]	σ (nm)[b]
$PTMC_{50}$-*b*-$PDLLA_{100}$-*b*-$PTMC_{50}$	Solvent evap. & Crosslink	45 %	110	40
$PTMC_{100}$-*b*-$PDLLA_{100}$-*b*-$PTMC_{100}$	Solvent evap. & Crosslink	60 %	120	30
$PTMC_{50}$-*b*-$PDLLA_{100}$-*b*-$PTMC_{50}$	SVA & Crosslink	42 %	120	40
$PTMC_{100}$-*b*-$PDLLA_{100}$-*b*-$PTMC_{100}$	SVA & Crosslink	58 %	170	40

[a] mean PDLLA domain size (n>80), [b] standard deviation

Unfortunately, the SAXS analysis of the photo-crosslinked films could not clearly provide a mean characteristic distance because of the q-range lower limit.

3.3.5 Study of the thermal and temporal stability of PTMC-b-PDLLA-b-PTMC self-assemblies

Optimized polymer diffusivity and increased mobility of the chains by thermal treatment has been employed for achieving phase-separated structures in differing block copolymer associations.[48, 49] However, the elevated thermal sensitivity of the amorphous PDLLA could possibly lead to premature degradation of the phase, and is something we wanted to investigate in our triblock copolymer systems**.** For that purpose, we precisely set the temperature at 65°C, being above the glass transition of both blocks.

As can be observed in the Figure 9A, such procedure did not improve the behavior on the blend polymers, where the samples tend to collapse completely under thermal influence, thus demonstrating that the block copolymer architecture, once again, presents bigger stability of the self-assembly. Nevertheless, as presented in Figure 9B, the photo-crosslinked *t*BCP thin film

started demonstrating an evolution of the morphology after 1 h exposure at 65°C, with average domain size of the PDLLA phase of 670 nm.

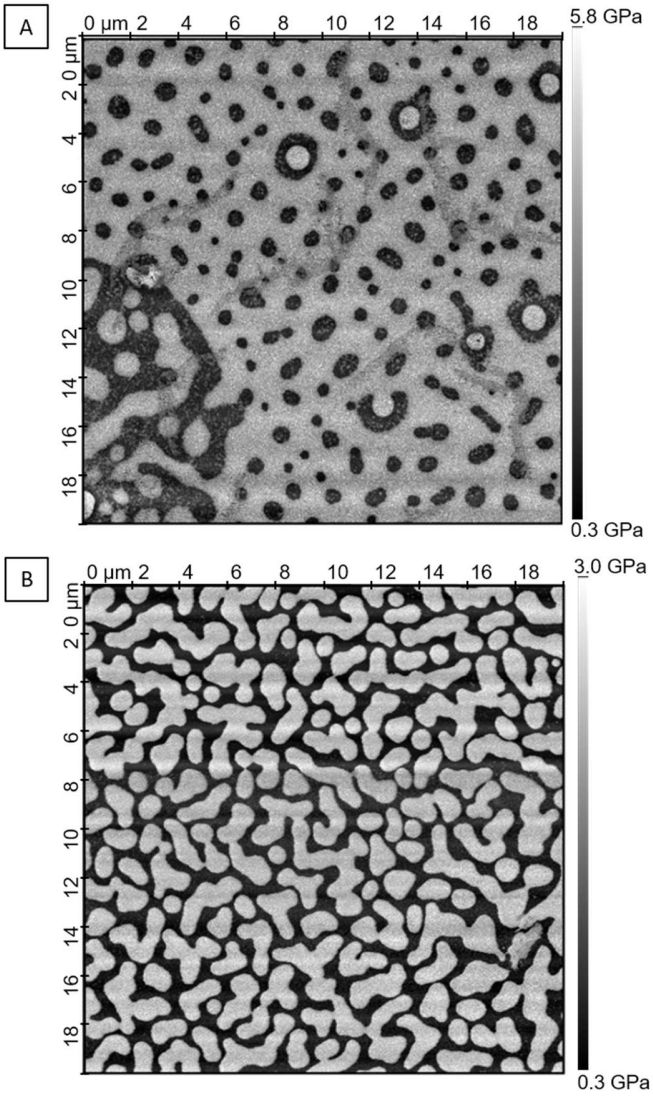

Figure 9. AFM thin film stiffness images of A) thermally annealed $PTMC_{100}$/$PDLLA_{100}$ blend; B) thermally annealed $PTMC_{50}$-*b*-$PDLLA_{100}$-*b*-$PTMC_{50}$ cured *t*BCP on 20 x 20 µm length scale. The white areas correspond to PDLLA (high modulus); the dark areas correspond to PTMC (low modulus).

A possible reason for such occurrence could be the PDLLA phase degradation, which provokes phase reorganization by the formation of a wetting surface on top of the film.[41] In fact, this phenomenon can result from the production of oligomers upon thermal degradation leading to a self-assembly destruction, thus provoking a complete reorganization of the structure once the PDLLA block is detached from the copolymer architecture.

To conclude, this thermal study demonstrates that the assemblies are stable up to temperatures neighboring the glass transition points of the system. Heating above the threshold point provokes a self-assembly reorganization and alters the phase-separated morphologies. Ideally, this system should be handled at temperatures no higher than 30°C.

On the other side, while discussing the stability in time of the samples when handled at temperatures below 30°C, the AFM images remained unchanged even upon 16 weeks (Figure S6). In this case, a chosen sample example of the cured $PTMC_{50}$-*b*-$PDLLA_{100}$-*b*-$PTMC_{50}$, after this time duration remained closely related to the one presented in Figure 5B.

3.4 Nanoporous PTMC thin films

In the aim to produce nanoporous templates, the highly ordered photo-crosslinked $PTMC_{100}$-*b*-$PDLLA_{100}$-*b*-$PTMC_{100}$ thin films resulting from solvent vapor annealing are the most suitable candidate for selective PDLLA etching due to their attractive bicontinuous morphology on a long-range 20 x 20 μm scale. Prior to any alkaline treatment on the copolymer film, we tested the treatment on pure PTMC film, which demonstrated no deterioration, hence a resistance of the PTMC to the alkaline treatment. Moreover, the fact that PTMC is the main part of the structure

(75 v/v%) which is further being reinforced by the stabilization from the photo-curing treatment, could favor the assurance of the porous system integrity.

Hence, after UV crosslinking, PDLLA hydrolysis and washing, the thin films were analyzed by DSC to confirm the selective PDLLA etching. Consequently, the cooling scan of this sample (Figure 10A) demonstrated a single glass transition temperature corresponding to the PTMC block (-16°C), justifying the successful PDLLA degradation and extraction of the by-products. Moreover, the glass transition point remained undeniably close to the one of PTMC in the triblock copolymer, demonstrating a resistance of the PTMC phase in the employed hydrolysis conditions.

Subsequently, the porosity of the sample was investigated by the means of SEM and TEM imaging. This type of imaging offers the possibility to determine the porous state of a system and especially the porous distribution within the film. Therefore, the SEM imaging (Figure 10B) demonstrated that the high degree of long-range order remained resistant upon hydrolysis. In fact, the staining contrast of the SEM imaging makes the PTMC phase appearing in bright, whereas instead of the PDLLA phase, interconnected cavities in the nanometer range scale are observable. In addition, in the aim to visualize the self-assembly efficiency inside the film, we performed TEM analyses of the film cross-section slice. Interestingly, the TEM image (Figure 10C) remarkably confirms that a 30 min alkaline solution treatment is efficient for effective PDLLA removal followed by nanosized pore generation within the entire film thickness that follows the phase organization present at the film top surface. In fact, in the TEM image of the porous sample, the porous cavities are neighboring the scale of 100 to 200 nm, similar to the average PDLLA domain size observable in the AFM images. However, it must be taken into consideration that in this case the imaging was performed in the interior of the sample and not

solely on its surface, alike in the AFM or SEM process. The calculations demonstrated a PTMC phase content of 66 % in the porous sample, hence 34 % of cavities, thus being in close relation to the initial proportions of both blocks in the triblock copolymer.

Moreover, these analyses were performed from the same Si-wafer support that the films were previously spin-coated onto, implicating their strong immobilization to the surface thanks to UV-photo-crosslinking. On the other side, the non-cured sample demonstrated insufficient mechanical resistance upon hydrolysis, visible by the film fracturing and delamination from the Si-wafer.

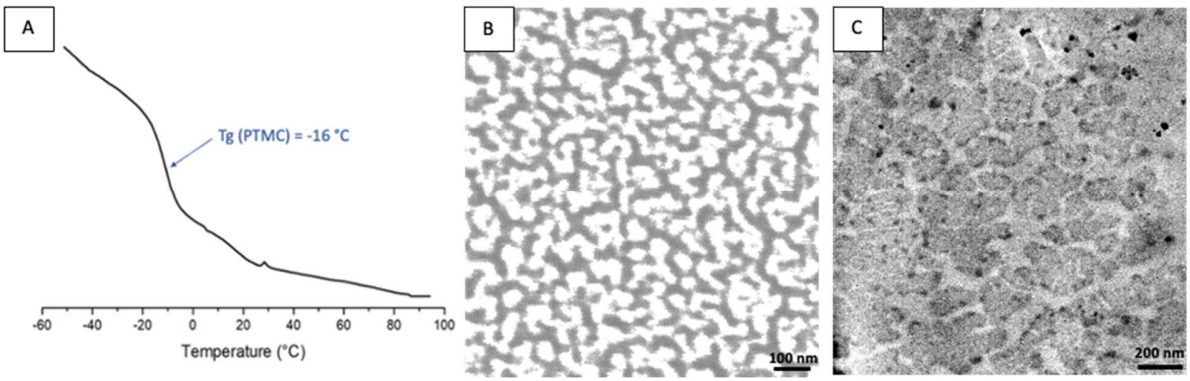

Figure 10. (A) DSC cooling scan of photo-crosslinked $PTMC_{100}$-*b*-$PDLLA_{100}$-*b*-$PTMC_{100}$ thin film after hydrolysis, (B) SEM image of the nanoporous PTMC thin film with a scale bar of 100 nm and (C) cross-section slice image by transmission electron micrograph (TEM) of the nanoporous PTMC thin film where the scale bar is 200 nm.

These advances represent an important contribution to the large area of block copolymer phase-separation and the production of nanoporous templates from biodegradable amorphous self-assembled associations. All at once, this study could represent the starting point to any future optimization of the PTMC-PDLLA self-assembly in terms of solvent vapor annealing, the choice

of solvents, impact of block copolymer lengths, etc. Taking into account the recognized PTMC biocompatibility, nanoporous PTMC systems would be greatly beneficial for biomedical application especially for tissue engineering scaffolds in order to improve the permeability, the nutrient adsorption performance and favored cell adhesion and growth.[50, 51] From another perspective, PTMC has recently been used as polymer electrolyte in Li-ion[52] or Na-ion[53] batteries, owing to its low Tg and good conductivity; thus, our nanoporous PTMC offers promising perspectives to design advanced composite electrolytes with bicontinous networks.

4. Conclusion

Nanoporous polymers generated by phase separation of biodegradable block copolymers have been scarcely studied up to day. In this article, we investigated such self-assembling phenomena in a carefully selected biodegradable block copolymer association. Theoretical studies on the PTMC-PDLLA interaction parameter let us expect a possible phase-separation in such system, which was further confirmed by DSC analysis. Their self-assembly was investigated in the thin-film geometry, produced by the spin-coating technique. Moreover, thin films photo-crosslinking employed towards porous matrix stabilization, did not disrupt the phase-separation of the system. Solvent vapor annealing resulted as the optimal annealing technique, leading to bicontinuous domains of nanoscopic PTMC and PDLLA phases on a long-length scale while employing triblock copolymer thin films, both before and after UV-curing. In contrast, the same annealing conditions did not result in ordered morphologies in the case of PTMC/PDLLA blends. The thin film presenting the most homogenized organization herein, once subjected to selective PDLLA etching upon hydrolysis, resulted in a nanoporous PTMC with a long range bicontinuous porous morphology. This investigation stands for the encouraging perspective of nanoporous

biodegradable materials and their possible application in various domains like the energy or biomedical ones.

ASSOCIATED CONTENT

Corresponding Author

* Sebastien Blanquer (sebastien.blanquer@umontpellier.fr)

Author Contributions

Nikola Toshikj: Investigation Methodology, Roles/Writing - original draft **Jason Richards**: Formal analysis, **Michel Ramonda**: Formal analysis, **Jean-Jacques Robin**: Supervision, Conceptualization **Sebastien Blanquer**: Supervision Conceptualization Writing - review & editing.

Funding Sources

The research work presented herein has been supported by the French Ministry of Higher Education and Research.

ACKNOWLEDGMENTS

The co-authors would like to thank Véronique Viguier and Erwan Oliviero from the platform of electronic microscopy (MEA) at the University of Montpellier for their contribution in the TEM analyses, and Philippe Dieudonné-George from the Charles Coulomb Laboratory for the SAXS analyses.

REFERENCES

[1] T.Y. Liu, G.L. Liu, Porous organic materials offer vast future opportunities, Nat Commun 11(1) (2020).
[2] D.C. Wu, F. Xu, B. Sun, R.W. Fu, H.K. He, K. Matyjaszewski, Design and Preparation of Porous Polymers, Chem Rev 112(7) (2012) 3959-4015.
[3] D.A. Olson, L. Chen, M.A. Hillmyer, Templating nanoporous polymers with ordered block copolymers, Chem Mater 20(3) (2008) 869-890.
[4] B. Le Droumaguet, R. Poupart, D. Grande, "Clickable" thiol-functionalized nanoporous polymers: from their synthesis to further adsorption of gold nanoparticles and subsequent use as efficient catalytic supports, Polym Chem-Uk 6(47) (2015) 8105-8111.
[5] F.S. Bates, G.H. Fredrickson, Block Copolymer Thermodynamics - Theory and Experiment, Annu Rev Phys Chem 41 (1990) 525-557.
[6] Y.Y. Mai, A. Eisenberg, Self-assembly of block copolymers, Chem Soc Rev 41(18) (2012) 5969-5985.
[7] F.S. Bates, G.H. Fredrickson, Block copolymers - Designer soft materials, Phys Today 52(2) (1999) 32-38.
[8] J.K. Kim, S.Y. Yang, Y. Lee, Y. Kim, Functional nanomaterials based on block copolymer self-assembly, Prog Polym Sci 35(11) (2010) 1325-1349.
[9] M.A. Hillmyer, Nanoporous materials from block copolymer precursors, Adv Polym Sci 190 (2005) 137-181.
[10] J.S. Lee, A. Hirao, S. Nakahama, Polymerization of Monomers Containing Functional Silyl Groups .5. Synthesis of New Porous Membranes with Functional-Groups, Macromolecules 21(1) (1988) 274-276.
[11] A.S. Zalusky, R. Olayo-Valles, J.H. Wolf, M.A. Hillmyer, Ordered nanoporous polymers from polystyrene-polylactide block copolymers, J Am Chem Soc 124(43) (2002) 12761-12773.
[12] M.S. She, T.Y. Lo, H.Y. Hsueh, R.M. Ho, Nanostructured thin films of degradable block copolymers and their applications, Npg Asia Mater 5 (2013).
[13] D. Grande, J. Penelle, P. Davidson, I. Beurroies, R. Denoyel, Functionalized ordered nanoporous polymeric materials: From the synthesis of diblock copolymers to their nanostructuration and their selective degradation, Micropor Mesopor Mat 140(1-3) (2011) 34-39.
[14] E.A. Jackson, Y. Lee, M.R. Radlauer, M.A. Hillmyer, Well-Ordered Nanoporous ABA Copolymer Thin Films via Solvent Vapor Annealing, Homopolymer Blending, and Selective Etching of ABAC Tetrablock Terpolymers, Acs Appl Mater Inter 7(49) (2015) 27331-27339.
[15] S. RameshKumar, P. Shaiju, K.E. O'Connor, P.R. Babu, Bio-based and biodegradable polymers - State-of-the-art, challenges and emerging trends, Curr Opin Green Sust 21 (2020) 75-81.
[16] K. Fukushima, Poly(trimethylene carbonate)-based polymers engineered for biodegradable functional biomaterials, Biomater Sci-Uk 4(1) (2016) 9-24.

[17] S. Schuller-Ravoo, J. Feijen, D.W. Grijpma, Preparation of Flexible and Elastic Poly(trimethylene carbonate) Structures by Stereolithography, Macromol Biosci 11(12) (2011) 1662-1671.
[18] T. Brossier, G. Volpi, J. Vasquez-Villegas, N. Petitjean, O. Guillaume, V. Lapinte, S. Blanquer, Photoprintable Gelatin-graft-Poly(trimethylene carbonate) by Stereolithography for Tissue Engineering Applications, Biomacromolecules 22(9) (2021) 3873-3883.
[19] M.A. Elsawy, K.H. Kim, J.W. Park, A. Deep, Hydrolytic degradation of polylactic acid (PLA) and its composites, Renew Sust Energ Rev 79 (2017) 1346-1352.
[20] T. Pasman, D. Baptista, S. van Riet, R.K. Truckenmuller, P.S. Hiemstra, R.J. Rottier, D. Stamatialis, A.A. Poot, Development of Porous and Flexible PTMC Membranes for In Vitro Organ Models Fabricated by Evaporation-Induced Phase Separation, Membranes-Basel 10(11) (2020).
[21] Y.Y. Qin, M.L. Yuan, L. Li, S.Y. Guo, M.W. Yuan, W. Li, J. Xue, Use of polylactic acid/polytrimethylene carbonate blends membrane to prevent postoperative adhesions, J Biomed Mater Res B 79b(2) (2006) 312-319.
[22] S. Zhang, H.L. Li, M.W. Yuan, M.L. Yuan, H.Y. Chen, Poly(Lactic Acid) Blends with Poly(Trimethylene Carbonate) as Biodegradable Medical Adhesive Material, Int J Mol Sci 18(10) (2017).
[23] N. Toshikj, J.J. Robin, S. Blanquer, A simple and general approach for the synthesis of biodegradable triblock copolymers by organocatalytic ROP from poly(lactide) macroinitiators, Eur Polym J 127 (2020).
[24] O. Sahin, S. Magonov, C. Su, C.F. Quate, O. Solgaard, An atomic force microscope tip designed to measure time-varying nanomechanical forces, Nat Nanotechnol 2(8) (2007) 507-514.
[25] H.S. Elbro, A. Fredenslund, P. Rasmussen, Group Contribution Method for the Prediction of Liquid Densities as a Function of Temperature for Solvents, Oligomers, and Polymers, Ind Eng Chem Res 30(12) (1991) 2576-2582.
[26] M.W. Matsen, F.S. Bates, Unifying weak- and strong-segregation block copolymer theories, Macromolecules 29(4) (1996) 1091-1098.
[27] I.M. Kalogeras, W. Brostow, Glass Transition Temperatures in Binary Polymer Blends, J Polym Sci Pol Phys 47(1) (2009) 80-95.
[28] L.M. Pitet, A.H.M. van Loon, E.J. Kramer, C.J. Hawker, E.W. Meijer, Nanostructured Supramolecular Block Copolymers Based on Polydimethylsiloxane and Polylactide, Acs Macro Lett 2(11) (2013) 1006-1010.
[29] J. Bang, S.H. Kim, E. Drockenmuller, M.J. Misner, T.P. Russell, C.J. Hawker, Defect-free nanoporous thin films from ABC triblock copolymers, J Am Chem Soc 128(23) (2006) 7622-7629.
[30] M. Vayer, M.A. Hillmyer, M. Dirany, G. Thevenin, R. Erre, C. Sinturel, Perpendicular orientation of cylindrical domains upon solvent annealing thin films of polystyrene-b-polylactide, Thin Solid Films 518(14) (2010) 3710-3715.
[31] J.L. Zhang, X.H. Yu, P. Yang, J. Peng, C.X. Luo, W.H. Huang, Y.C. Han, Microphase Separation of Block Copolymer Thin Films, Macromol Rapid Comm 31(7) (2010) 591-608.
[32] E. Han, K.O. Stuen, M. Leolukman, C.C. Liu, P.F. Nealey, P. Gopalan, Perpendicular Orientation of Domains in Cylinder-Forming Block Copolymer Thick Films by Controlled Interfacial Interactions, Macromolecules 42(13) (2009) 4896-4901.
[33] C. Sinturel, M. Vayer, M. Morris, M.A. Hillmyer, Solvent Vapor Annealing of Block Polymer Thin Films, Macromolecules 46(14) (2013) 5399-5415.

[34] J.M. Leiston-Belanger, T.P. Russell, E. Drockenmuller, C.J. Hawker, A thermal and manufacturable approach to stabilized diblock copolymer templates, Macromolecules 38(18) (2005) 7676-7683.
[35] P. Nguyen-Tri, P. Ghassemi, P. Carriere, S. Nanda, A.A. Assadi, D.D. Nguyen, Recent Applications of Advanced Atomic Force Microscopy in Polymer Science: A Review, Polymers-Basel 12(5) (2020).
[36] W.A. Phillip, M.A. Hillmyer, E.L. Cussler, Cylinder Orientation Mechanism in Block Copolymer Thin Films Upon Solvent Evaporation, Macromolecules 43(18) (2010) 7763-7770.
[37] S.H. Kim, M.J. Misner, T. Xu, M. Kimura, T.P. Russell, Highly oriented and ordered arrays from block copolymers via solvent evaporation, Adv Mater 16(3) (2004) 226-231.
[38] D. Garlotta, A literature review of poly(lactic acid), J Polym Environ 9(2) (2001) 63-84.
[39] A.P. Pego, D.W. Grijpma, J. Feijen, Enhanced mechanical properties of 1,3-trimethylene carbonate polymers and networks, Polymer 44(21) (2003) 6495-6504.
[40] A. Baruth, M. Seo, C.H. Lin, K. Walster, A. Shankar, M.A. Hillmyer, C. Leighton, Optimization of Long-Range Order in Solvent Vapor Annealed Poly(styrene)-block-poly(lactide) Thin Films for Nano lithography, Acs Appl Mater Inter 6(16) (2014) 13770-13781.
[41] K.A. Cavicchi, T.P. Russell, Solvent annealed thin films of asymmetric polyisoprene-polylactide diblock copolymers, Macromolecules 40(4) (2007) 1181-1186.
[42] M.A. Chavis, D.M. Smilgies, U.B. Wiesner, C.K. Ober, Widely Tunable Morphologies in Block Copolymer Thin Films Through Solvent Vapor Annealing Using Mixtures of Selective Solvents, Adv Funct Mater 25(20) (2015) 3057-3065.
[43] C. Jin, B.C. Olsen, E.J. Luber, J.M. Buriak, Nanopatterning via Solvent Vapor Annealing of Block Copolymer Thin Films, Chem Mater 29(1) (2017) 176-188.
[44] Y. Xuan, J. Peng, L. Cui, H.F. Wang, B.Y. Li, Y.C. Han, Morphology development of ultrathin symmetric diblock copolymer film via solvent vapor treatment, Macromolecules 37(19) (2004) 7301-7307.
[45] C.G. Gamys, J.M. Schumers, A. Vlad, C.A. Fustin, J.F. Gohy, Amine-functionalized nanoporous thin films from a poly(ethylene oxide)-block-polystyrene diblock copolymer bearing a photocleavable o-nitrobenzyl carbamate junction, Soft Matter 8(16) (2012) 4486-4493.
[46] T. Ito, H. Coceancigh, Y. Yi, J.N. Sharma, F.C. Parks, A.H. Flood, Nanoporous Thin Films Formed from Photocleavable Diblock Copolymers on Gold Substrates Modified with Thiolate Self-Assembled Monolayers, Langmuir 36(31) (2020) 9259-9268.
[47] F. Zhang, J. Ilavsky, Ultra-Small-Angle X-ray Scattering of Polymers, Polym Rev 50(1) (2010) 59-90.
[48] K.W. Guarini, C.T. Black, S.H.I. Yeuing, Optimization of diblock copolymer thin film self assembly, Adv Mater 14(18) (2002) 1290-+.
[49] R. Olayo-Valles, S.W. Guo, M.S. Lund, C. Leighton, M.A. Hillmyer, Perpendicular domain orientation in thin films of polystyrene - Polylactide diblock copolymers, Macromolecules 38(24) (2005) 10101-10108.
[50] Z.Q. Dong, H.J. Cui, H.D. Zhang, F. Wang, X. Zhan, F. Mayer, B. Nestler, M. Wegener, P.A. Levkin, 3D printing of inherently nanoporous polymers via polymerization-induced phase separation, Nat Commun 12(1) (2021).
[51] H.B. Ly, B. Le Droumaguet, V. Monchiet, D. Grande, Tailoring doubly porous poly(2-hydroxyethyl methacrylate)-based materials via thermally induced phase separation, Polymer 86 (2016) 138-146.

[52] J.J. Zhang, J.F. Yang, T.T. Dong, M. Zhang, J.C. Chai, S.M. Dong, T.Y. Wu, X.H. Zhou, G.L. Cui, Aliphatic Polycarbonate-Based Solid-State Polymer Electrolytes for Advanced Lithium Batteries: Advances and Perspective, Small 14(36) (2018).
[53] C. Sangeland, R. Younesi, J. Mindemark, D. Brandell, Towards room temperature operation of all-solid-state Na-ion batteries through polyester-polycarbonate-based polymer electrolytes, Energy Storage Mater 19 (2019) 31-38.

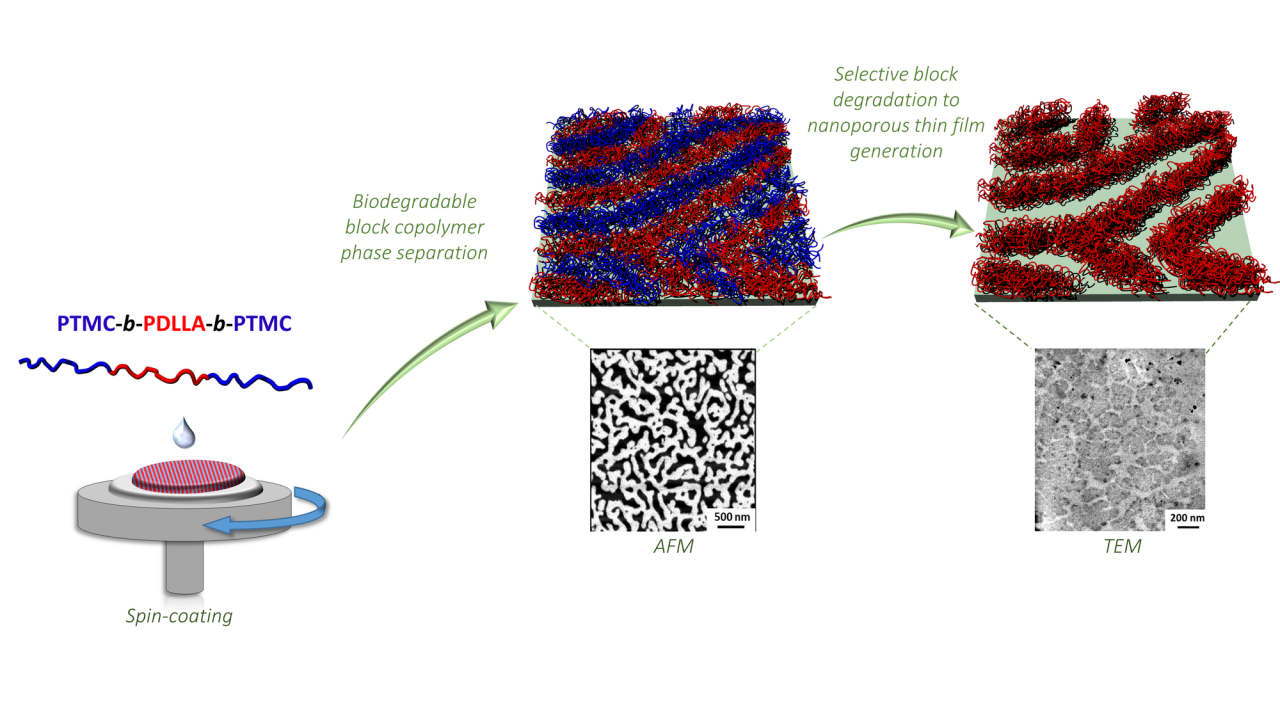
PTMC-b-PDLLA-b-PTMC
Spin-coating
Biodegradable block copolymer phase separation
500 nm
AFM
Selective block degradation to nanoporous thin film generation
200 nm
TEM